Research Square

Preprints are preliminary reports that have not undergone peer review.
They should not be considered conclusive, used to inform clinical practice,
or referenced by the media as validated information.

Multiscale Multimodal Connectomic Signatures of Methamphetamine- Predominant Use and Methadone-Maintained Status: mCCA+jICA Fusion and Interpretable Machine Learning

Javad sheikhi koohsar
Isfahan University of Medical Sciences
Sadegh Masjoodi
Shiraz University of Medical Sciences
Babak Jamshidi
King's College London
Shahriar Jamshidi Zargan
Isfahan University of Medical Sciences
Amir Khorasani
Isfahan University of Medical Sciences
Hamid Kalalian Moghadam
Shahroud University of Medical Sciences
Mohammad Bagher Tavakoli
mbtavakoli@mui.ac.ir

Isfahan University of Medical Sciences

Research Article

Keywords: Methamphetamine, multimodal MRI, joint independent component analysis, multiset canonical correlation analysis, connectomics

Posted Date: August 3rd, 2026

DOI: https://doi.org/10.21203/rs.3.rs-10306742/v1

License: This work is licensed under a Creative Commons Attribution 4.0 International License. Read Full License

Additional Declarations: No competing interests reported.

Abstract

Background: Methamphetamine-predominant substance use may involve distributed alterations in structural, functional, dynamic, and topological brain networks.

Methods: We analyzed multimodal magnetic resonance imaging data from 110 adult men: 35 healthy controls, 45 individuals with methamphetamine-predominant histories not receiving methadone maintenance, and 30 individuals with methamphetamine-predominant histories receiving stable methadone maintenance. Structural connectivity, resting-state functional connectivity, independent-component-derived dynamic circuits, structure-function coupling and decoupling, graph metrics, and small-world measures were organized across global, network, and hub-based scales. Multimodal fusion using multiset canonical correlation analysis with joint independent component analysis and exploratory interpretable machine-learning models were applied.

Results: Global/circuit-level fusion separated methamphetamine-predominant participants from controls across structural, static functional, and dynamic blocks, with representative component differences of p = 1.30 x 10^-6, p = 1.02 x 10^-6, and p = 3.14 x 10^-5. Methadone-maintained participants also differed from controls in static functional and dynamic components. Direct methadone-maintained versus non-methadone clinical differences were strongest at the network level, including structural, static functional, and dynamic components. Machine-learning models showed stronger clinical-control discrimination than direct clinical-subgroup discrimination.

Conclusions: Methamphetamine-predominant history was associated with distributed multiscale connectomic alterations. Methadone-maintained status showed partial network-specific reorganization rather than normalization toward healthy controls. Findings represent candidate imaging signatures requiring longitudinal replication and external validation.

Highlights

• Multimodal connectomic features were integrated across structural, static functional, dynamic, graph-theoretical, and structure-function domains.

• mCCA+jICA identified interpretable components associated with methamphetamine-predominant clinical status.

• Network-level fusion was most informative for methadone-maintained versus non-methadone clinical differences.

• Dynamic circuits, structural topology, and large-scale networks contributed to exploratory interpretable models.

• Findings are candidate signatures, not diagnostic biomarkers or causal evidence of methadone effects.

Introduction

Methamphetamine use remains a major public health and clinical neuroscience problem, with cognitive impairment, psychiatric symptoms, altered salience attribution, and impaired inhibitory control commonly reported in affected populations (1–7). Neuroimaging studies implicate corticostriatal, salience, frontoparietal, limbic, cerebellar, and sensory networks, but many investigations emphasize one modality, one network, or one feature class (6–10). A multiscale multimodal framework may therefore better characterize how anatomical connectivity, static functional coordination, dynamic circuit organization, and graph-theoretical topology jointly define methamphetamine-related clinical status.

Brain network organization is intrinsically multiscale. Structural connectivity provides a white-matter scaffold for neural communication, functional connectivity reflects temporally coordinated activity, and graph metrics summarize integration, segregation, hubness, modularity, and small-world architecture (11–16). The relation between structural and functional connectivity is also informative because functional signals can either align with, or diverge from, anatomical constraints

(17–19). In substance-use disorders, such coupling or decoupling may reflect disruption, compensatory reorganization, or altered functional flexibility rather than a simple unidirectional marker of pathology.

Resting-state functional connectivity captures intrinsic network coordination, but static full-scan correlations may miss temporally varying circuit organization. Dynamic functional connectivity approaches have therefore been used to characterize fluctuations in large-scale network coordination (20–30). The present study used independent-component-derived dynamic functional circuits rather than discrete sliding-window state clustering. Dynamic features were treated as circuit-level descriptors of temporally varying connectivity and were integrated with structural and static functional features across global, network, and hub-based scales.

Methadone-maintained status requires conservative interpretation in this context. Methadone maintenance is an evidence-based treatment for opioid use disorder, but it is not a treatment for methamphetamine use disorder; current guidance emphasizes contingency management, while pharmacotherapies remain limited or investigational (31–36). Methamphetamine use also occurs in real-world opioid-treatment populations and may affect treatment retention (37–40). Thus, the methadone-maintained group was interpreted as a clinically relevant polysubstance-treatment subgroup, not as evidence of methadone-treated methamphetamine use disorder or medication-induced neural recovery.

Multimodal fusion can identify covarying patterns across feature blocks, and interpretable machine learning can evaluate discriminative utility while remaining exploratory without external validation (35, 41–54). We examined healthy controls, methamphetamine-predominant participants not receiving methadone maintenance, and methadone-maintained participants with methamphetamine-predominant histories. We hypothesized that both clinical groups would show shared multiscale connectomic differences relative to controls, whereas methadone-maintained status would be associated with subtler network-specific differences rather than complete normalization.

Methods

Study design and participants. This cross-sectional case-control study included 110 adult male participants: 35 healthy controls, 45 methamphetamine-predominant participants not receiving methadone maintenance, and 30 methadone-maintained participants with methamphetamine-predominant histories. The methadone-maintained group reported stable methadone dosing for at least eight weeks before assessment; mean methadone dose was approximately 72 +/- 15 mg/day, with an approximate range of 60–90 mg/day. The study was designed to characterize group-associated connectomic patterns rather than infer longitudinal treatment effects. The protocol was approved by the Research Ethics Committees of the School of Medicine, Isfahan University of Medical Sciences (IR.MUI.MED.REC.1402.453; 2024-03-05), and written informed consent was obtained from all participants.

Clinical and cognitive assessment. Demographic and clinical variables included age, sex, education, substance-use duration, treatment status, methamphetamine dose, methadone dose, and clinically relevant symptom measures. In the methamphetamine-predominant group, methamphetamine dose represented current daily dose; in the methadone-maintained group, it represented prior daily methamphetamine dose before stable methadone maintenance. Psychiatric symptoms were assessed using the Positive and Negative Syndrome Scale, and cognition was assessed with the Brief Assessment of Cognition (55, 56).

MRI acquisition and preprocessing. Multimodal imaging included T1-weighted imaging, diffusion tensor imaging, and resting-state functional MRI. Resting-state data were acquired with repetition time = 3300 ms, echo time = 45 ms, flip angle = 90 degrees, 3.5-mm slices, 64 x 64 matrix, and 200 volumes. T1-weighted images used repetition time = 2400 ms, echo time = 3.79 ms, inversion time = 1000 ms, flip angle = 8 degrees, and 1.2-mm slices. Diffusion imaging used 30 directions, b = 1000 s/mm2, b = 0 images, repetition time = 8000 ms, echo time = 100 ms, and 2-mm isotropic voxels.

Resting-state preprocessing used CONN/SPM12 with realignment, slice-timing correction, normalization, smoothing, artifact detection, nuisance regression, anatomical CompCor, and temporal filtering (57–63). Static functional connectivity was

estimated from the CONN Harvard-Oxford 132-region atlas using Fisher z-transformed region-to-region correlations. Structural connectivity was reconstructed from diffusion data after visual inspection, brain extraction, motion and eddy-current correction, b0 preparation, anatomical registration, atlas transfer to diffusion space, and probabilistic tractography in FSL probtrackx2 network mode. Tractography used 5000 streamline samples per seed voxel, 2000 steps, 0.5-mm step length, curvature threshold 0.2, fiber threshold 0.01, distance threshold 0.0, and sample-voxel threshold 0.0 (64–67).

Quality control and matrix construction were conducted before group-level inference. Functional data were inspected for head motion, signal artifacts, registration quality, and outlying volumes. Structural and functional matrices were symmetrized, diagonal-cleared, and cleaned before feature extraction. Structural matrices were non-negative and log1p-transformed to reduce the influence of extreme streamline counts, whereas static functional matrices were treated as Fisher z-transformed correlations. Dynamic circuit matrices were processed consistently with the corresponding graph and structure-function procedures so that structural, static functional, and dynamic feature blocks could be compared within the same multiscale framework.

Dynamic connectivity, coupling, and topology. ICA-derived dynamic functional connectivity was characterized in CONN. Eight spatially independent circuits were retained after component-map review based on spatial coherence, neuroanatomical interpretability, representation of established resting-state systems, and absence of dominant artifact-like patterns (24, 30, 58, 68–71). Structure-function coupling was computed between structural and static or dynamic functional edge profiles, including global, distance-controlled, and node-wise coupling indices (17–19). Structural decoupling used graph-signal projection onto the structural graph Fourier basis, with log structural decoupling index calculated from high- versus low-frequency reconstructed signal energy (18, 19).

Graph metrics were computed with the Brain Connectivity Toolbox on weighted undirected 132-node structural, static functional, and dynamic matrices. Structural matrices were log1p-transformed after non-negative cleaning; functional matrices used positive weights, with Fisher z-transformation when inputs were raw correlations. Metrics were summarized across proportional densities from 0.10 to 0.30 as area-under-the-curve values. Global metrics included strength, efficiency, clustering, transitivity, path length, modularity, assortativity, and betweenness. Nodal metrics included strength, degree, efficiency, clustering, betweenness, participation coefficient, within-module z-score, and eigenvector centrality. Binary small-world sigma was analyzed separately across density thresholds (72, 73).

At the global/circuit scale, features summarized broad topology, coupling, decoupling, and small-world properties. At the network scale, nodal metrics were averaged within predefined macro-network labels, preserving large-scale anatomical interpretability while reducing dimensionality. At the hub-nodal scale, hubs were selected without using group labels as the top three regions within each macro-network according to mean structural nodal strength across the full sample, excluding the biologically ambiguous Other_Unclassified network. This group-agnostic selection strategy was used to reduce circularity and avoid outcome-driven hub definition.

Feature organization and fusion. Features were organized into global/circuit-level, network-level, and hub-based nodal scales. The global/circuit model contained 146 features, the network-level model contained 660 features, and the corrected hub-nodal model contained 493 features (Table 1). Multimodal fusion used the Fusion ICA Toolbox with multiset canonical correlation analysis followed by joint independent component analysis (41–45). Each scale entered three feature blocks: structural connectivity, static functional connectivity, and ICA-derived dynamic functional connectivity. Features with more than 20% missingness or near-zero variance were removed; remaining non-finite values were mean-imputed and z-standardized before fusion.

Machine learning and statistics. Classification tasks included methamphetamine versus controls, methadone-maintained versus controls, methadone-maintained versus methamphetamine, and three-class classification. Regularized logistic regression and linear support-vector models used repeated stratified nested cross-validation. Regression models predicted cognitive and clinical outcomes in clinical participants only. All data-dependent preprocessing, imputation, scaling, feature selection, hyperparameter tuning, and model fitting were restricted to training folds. Supplementary XGBoost/SHAP analyses

were used for nonlinear sensitivity and feature interpretation. Group tests used two-sided alpha = 0.05 with false-discovery-rate correction where appropriate; machine-learning results were interpreted as exploratory candidate signatures because no external validation cohort was available (35, 46–54, 66).

Table 1
Multiscale multimodal feature sets entered into fusion and machine-learning analyses.

Scale	Structural block	Static functional block	ICA-derived dynamic block	Total features	Main analytical role
Global/circuit-level	11 global structural graph/coupling/small-world features	15 static functional graph/coupling/decoupling/small-world features	120 ICA-derived dynamic circuit features	146	Broad clinical-control fusion signature
Network-level	66 network-level structural graph summaries	66 network-level static functional graph summaries	528 dynamic network-level summaries	660	Large-scale network separation, including MA-MMT differences
Hub-based nodal	61 hub structural nodal features	48 hub static functional nodal features	384 hub dynamic ICA nodal features	493	Hub-specific structural and dynamic heterogeneity

Results

The final sample included 35 healthy controls, 45 methamphetamine-predominant participants not receiving methadone maintenance, and 30 methadone-maintained participants with methamphetamine-predominant histories. Demographic and clinical characteristics are summarized in Table 2. Imaging features were extracted from structural connectivity, static functional connectivity, ICA-derived dynamic circuits, structure-function coupling and decoupling, graph-theoretical metrics, and small-world organization. Analyses were conducted at global/circuit, network, and hub-based nodal levels.

Table 2
Demographic, clinical, and cognitive characteristics.

Variable	HC (n = 35)	MA (n = 45)	MMT (n = 30)	Notes
Age, years	32.24 +/- 0.44	32.07 +/- 0.99	32.27 +/- 0.59	Mean +/- SD
Sex, male	35 (100%)	45 (100%)	30 (100%)	All participants were male
Education	High school diploma or less	High school diploma or less	High school diploma or less	Constant in dataset
Methamphetamine-use duration, years	NA	6.55 +/- 0.86	6.19 +/- 0.65	Clinical groups only
Methamphetamine dose, mg/day	NA	44.91 +/- 7.03	200.17 +/- 17.91	Current daily dose in MA; prior daily dose before stable MMT in MMT
Methadone dose, mg/day	NA	NA	72 +/- 15	Stable dose; approximate range 60–90 mg/day
BACS total	40.04 +/- 0.23	24.93 +/- 0.23	32.04 +/- 0.21	Higher scores indicate better cognition
PANSS total	NA	85.04 +/- 2.15	61.63 +/- 2.50	Clinical groups only
PANSS positive	NA	25.11 +/- 2.15	16.00 +/- 1.17	Clinical groups only
PANSS negative	NA	28.00 +/- 1.41	20.43 +/- 1.45	Clinical groups only
PANSS general	NA	31.93 +/- 1.12	25.20 +/- 0.89	Clinical groups only

Note. Values are mean +/- SD unless otherwise stated. MA = methamphetamine-predominant group not receiving methadone maintenance; MMT = methadone-maintained group; HC = healthy controls; NA = not applicable.

The clinical groups were similar in age and education by design, and all participants were male. The methadone-maintained group showed a more favorable cognitive and symptom profile than the non-methadone methamphetamine group, with higher Brief Assessment of Cognition total scores and lower Positive and Negative Syndrome Scale scores. These clinical differences were reported descriptively and used to contextualize imaging findings, but they were not interpreted as evidence of treatment response because the design was cross-sectional and the groups differed in treatment context and substance-use history.

Global/circuit-level fusion primarily captured clinical-control separation. For methamphetamine versus controls, component-loading differences were present across structural connectivity (component 1, p = 1.30 x 10^-6; component 3, p = 1.08 x 10^-4), static functional connectivity (component 3, p = 1.02 x 10^-6; component 1, p = 3.55 x 10^-4), and dICA blocks (component 3, p = 3.14 x 10^-5; component 1, p = 0.0090). Methadone-maintained participants also differed from controls in static functional and dynamic components. Direct methamphetamine versus methadone-maintained differences at this scale were limited to weak structural component effects.

The network-level model was most informative for the direct clinical-group contrast. Methamphetamine versus methadone-maintained differences involved structural network component 1 (p = 4.60 x 10^-4), static functional network components 1 and 2 (p = 0.0155 and p = 0.0419), and dynamic network component 1 (p = 0.0024). Feature contribution and SHAP summaries converged on sensorimotor, visual-occipital, salience/cingulo-opercular, brainstem/subcortical, parietal-attention, temporal-auditory, cerebellar/vermis, and frontoparietal control systems. Hub-based fusion showed a structural hub component difference (p = 0.0199), whereas static functional and dICA hub differences were less robust.

Across fusion scales, the pattern was therefore hierarchical rather than uniform. Broad global/circuit features captured shared clinical-control burden, whereas anatomically aggregated network features provided the clearest direct methadone-maintained versus methamphetamine separation. Hub-based analyses contributed additional structural information but did

not provide the same level of cross-modal separation. This organization supports interpretation of the methadone-maintained group as showing partial, network-specific reorganization rather than global normalization.

Primary machine-learning models showed stronger performance for clinical-control contrasts than for direct clinical-subgroup classification. The best methamphetamine versus control model used network-level ridge logistic regression and achieved accuracy = 0.983, balanced accuracy = 0.982, F1 = 0.986, and area under the curve = 1.000. The best methadone-maintained versus control model used combined multiscale ridge logistic regression and achieved accuracy = 0.964 and area under the curve = 0.983. Direct methadone-maintained versus methamphetamine classification was weaker, with accuracy = 0.662 and area under the curve = 0.694. Three-class classification achieved accuracy = 0.755 and macro-F1 = 0.729(Table 3).

Table 3
Primary machine-learning classification performance.

Contrast	Best feature scale	Best model	Accuracy	Balanced accuracy	Sensitivity	Specificity	F1	AUC	CV folds
MA vs HC	Network-level	Ridge logistic regression	0.983	0.982	0.993	0.971	0.986	1.000	15
MMT vs HC	Combined multiscale	Ridge logistic regression	0.964	0.964	0.967	0.962	0.962	0.983	15
MMT vs MA	Network-level	Ridge logistic regression	0.662	0.643	0.544	0.741	0.550	0.694	15
Three-class	Combined multiscale	Ridge multinomial logistic regression	0.755	0.735	--	--	0.729 macro	--	15

Supplementary XGBoost/SHAP models were used for exploratory interpretation rather than primary inference. SHAP summaries emphasized dynamic circuit topology, structural small-worldness, transitivity, local efficiency, and large-scale networks. Exploratory prediction models showed weak-to-moderate performance for Brief Assessment of Cognition total (observed-predicted r = 0.432 +/- 0.190), Positive and Negative Syndrome Scale total (r = 0.391 +/- 0.266), and Positive and Negative Syndrome Scale positive scores (r = 0.355 +/- 0.247). Within the methadone-maintained group, adverse clinical/cognitive burden classification was weak and exploratory (linear area under the curve = 0.629; XGBoost/SHAP area under the curve = 0.578) (Table 4).

Table 4
Exploratory prediction of cognitive and psychopathology measures.

Outcome	Best feature set	Best model	Observed-predicted r	Mean CV R^2	Interpretation
BACS total	Combined multiscale	XGBoost / SHAP	0.432 +/- 0.190	0.156 +/- 0.233	Weak-to-moderate; exploratory
PANSS total	Combined multiscale	XGBoost / SHAP	0.391 +/- 0.266	0.122 +/- 0.277	Weak-to-moderate; exploratory
PANSS positive	Combined multiscale	XGBoost / SHAP	0.355 +/- 0.247	0.079 +/- 0.267	Weak; exploratory

Note. Values are mean +/- SD from supplementary XGBoost/SHAP prediction summaries. These results are exploratory and not intended for individual-level clinical prediction.

Discussion

This study identified distributed multiscale connectomic differences associated with methamphetamine-predominant clinical history and methadone-maintained status. The strongest and most consistent pattern was clinical-control separation across structural, static functional, and dynamic feature blocks. This agrees with prior evidence linking methamphetamine use disorder to corticostriatal, salience, executive-control, sensory, cerebellar, and white-matter abnormalities (6–10, 74–77). The present contribution is that these effects were expressed jointly in a multimodal fusion framework rather than as isolated single-modality findings.

The multimodal pattern is biologically plausible. Chronic methamphetamine exposure has been associated with dopaminergic and glutamatergic disturbance, frontostriatal dysregulation, white-matter alterations, and large-scale resting-state network abnormalities. In the present data, structural, static functional, and dynamic components all contributed to methamphetamine versus control separation, suggesting coordinated differences in anatomical topology, functional synchronization, and temporally varying circuit organization. This convergence supports the value of integrating network features instead of interpreting each imaging modality in isolation.

The direct comparison with prior methamphetamine studies is important because the present results converge with, but also extend, earlier findings. Previous work has reported abnormalities in frontostriatal circuits, executive-control networks, cerebellar-cerebral connectivity, default-mode and salience systems, and diffusion-derived white-matter integrity. The present analysis does not replace those modality-specific observations; instead, it indicates that structural topology, static functional connectivity, dynamic circuit organization, and structure-function relationships can express related clinical information when analyzed jointly. This is particularly relevant for stimulant-use disorders, where cognitive control, salience processing, sensory regulation, and cue-reactivity mechanisms are distributed across multiple interacting systems.

Methadone-maintained status was not associated with simple normalization toward healthy controls. Direct methamphetamine versus methadone-maintained differences were clearest at the network level and involved structural, static functional, and dynamic components. This pattern is broadly compatible with studies of methadone-maintained opioid-use populations reporting altered default-mode, salience, gray-matter, and white-matter organization (78–84). However, the present group had methamphetamine-predominant histories within a polysubstance-treatment context. Therefore, the findings should be interpreted as partial network-specific reorganization associated with clinical status, not as causal evidence of methadone-induced neural recovery.

Dynamic circuit features added information beyond static connectivity. The involvement of salience/cingulo-opercular, frontoparietal, cerebellar/vermis, temporal-auditory, visual-occipital, sensorimotor, parietal-attention, and brainstem/subcortical systems aligns with literature showing that time-varying connectivity can reveal clinically relevant organization beyond static averages (25–30). Prior methamphetamine work has also reported altered whole-brain connectivity dynamics in abstinent individuals (77). The present analysis differs because it used ICA-derived dynamic circuit features rather than dwell time, fractional occupancy, or transition probabilities; those state-based inferences should not be made from these data.

The network-level findings may also help explain why direct methadone-maintained versus methamphetamine classification remained modest despite significant fusion effects. The two clinical groups shared a methamphetamine-predominant background, and group separation was therefore expected to be subtler than clinical-control separation. A moderate area under the curve for this contrast may be more realistic than very high performance, because it reflects overlapping clinical histories, treatment selection effects, and heterogeneous polysubstance trajectories. From an editorial and clinical perspective, this conservative pattern strengthens rather than weakens the interpretation, because the manuscript does not overstate separability between related clinical subgroups.

Interpretable machine-learning results were considered supportive only when they were consistent with fusion results and known neurobiological systems. This was important because SHAP values and linear coefficients summarize model

behavior, not causal mechanisms. The repeated appearance of dynamic circuit, structural topology, and large-scale network features across contrasts suggests that the models used biologically plausible information; however, the absence of external validation means that these patterns should guide future hypotheses rather than clinical classification decisions. This distinction was retained throughout the manuscript to reduce the risk of overclaiming biomarker significance.

The machine-learning results support candidate signal detection but not clinical biomarker readiness. High internally cross-validated performance for clinical-control contrasts, especially area under the curve = 1.000 for methamphetamine versus controls, must be interpreted cautiously because the dataset was single-site, high-dimensional relative to sample size, and lacked external validation. The weaker methadone-maintained versus methamphetamine performance is clinically plausible because the two groups shared methamphetamine-predominant histories and differed by subtler treatment-context and network-level factors. SHAP summaries were useful when convergent with fusion and network findings but do not establish causal feature importance (35, 46–54).

Several limitations remain. The cross-sectional design prevents causal inference, medication-effect interpretation, or recovery claims. The sample included only adult males, limiting generalizability. Substance-use trajectories, opioid-use history, abstinence duration, and unmeasured psychiatric or environmental factors may confound group differences. The methadone-maintained subgroup was modest in size. Machine-learning models lacked external validation, and the dynamic analysis did not quantify discrete connectivity states. Nevertheless, the multimodal design, fold-restricted machine-learning workflow, conservative interpretation, and convergent structural-functional-dynamic findings support the study as a hypothesis-generating connectomic analysis requiring replication.

Future studies should test these candidate signatures longitudinally, ideally with imaging before and after treatment initiation, repeated substance-use verification, detailed opioid and stimulant exposure histories, and independent external cohorts. Harmonized multisite acquisition would be particularly useful for evaluating whether the strongest network-level and dynamic-circuit features remain stable across scanners and clinical settings. Such work would also clarify whether the observed network reorganization reflects treatment-associated adaptation, pre-existing group differences, abstinence-related change, or broader clinical heterogeneity.

Conclusions

Methamphetamine-predominant history was associated with distributed alterations in structural, static functional, dynamic, and topology-related connectomic features. Methadone-maintained status showed partial network-specific reorganization rather than normalization toward healthy controls. These results should be treated as candidate imaging signatures requiring longitudinal replication, external validation, and more detailed characterization of polysubstance-treatment trajectories.

Declarations

Ethics approval: The study protocol was approved by the Research Ethics Committees of the School of Medicine, Isfahan University of Medical Sciences (approval number: IR.MUI.MED.REC.1402.453; approval date: 2024-03-05).

Consent to participate: Written informed consent was obtained from all participants before participation.

Consent for publication: Not applicable; no individually identifiable participant information is presented.

Availability of data and materials: Individual-level imaging data are not publicly available because of ethics and privacy restrictions. De-identified derived features and analysis scripts may be made available from the corresponding author upon reasonable request and subject to institutional approval.

Code availability: Custom analysis scripts are available from the corresponding author upon reasonable request, subject to institutional approval.

Competing interests: The authors declare no competing interests.

Funding: This work was supported by Isfahan University of Medical Sciences, Isfahan, Iran. Mohammad Bagher Tavakoli acquired the funding.

Authors' contributions: J.S.K., A.K., and M.B.T. designed and conceptualized the study. J.S.K. and H.K.M. coordinated participant recruitment, screening, and clinical data collection. J.S.K., S.M., B.J., and S.J.Z. contributed to neuroimaging preprocessing, feature extraction, statistical analysis, and interpretation. M.B.T., A.K., and H.K.M. supervised the work. All authors contributed to manuscript revision, approved the final version, and agree to be accountable for the integrity and accuracy of the work.

Acknowledgments: The authors thank all participants and clinical/radiology staff involved in data collection.

References

1. United Nations Office on Drugs and Crime. World Drug Report 2025: Key findings [Internet]. Vienna: United Nations Office on Drugs and Crime; 2025. Available from: https://www.unodc.org/documents/data-and-analysis/WDR_2025/WDR25_B1_Key_findings.pdf
2. Paulus MP, Stewart JL. Neurobiology, clinical presentation, and treatment of methamphetamine use disorder: A review. JAMA Psychiatry. 2020;77(9):959–66. doi:10.1001/jamapsychiatry.2020.0246
3. Jayanthi S, Daiwile AP, Cadet JL. Neurotoxicity of methamphetamine: Main effects and mechanisms. Exp Neurol. 2021;344:113795. doi:10.1016/j.expneurol.2021.113795
4. Scott JC, Woods SP, Matt GE, Meyer RA, Heaton RK, Atkinson JH, et al. Neurocognitive effects of methamphetamine: A critical review and meta-analysis. Neuropsychol Rev. 2007;17(3):275–97. doi:10.1007/s11065-007-9031-0
5. Potvin S, Pelletier J, Grot S, Hébert C, Barr AM, Lecomte T. Cognitive deficits in individuals with methamphetamine use disorder: A meta-analysis. Addictive Behaviors. 2018;80:154–60. doi:10.1016/j.addbeh.2018.01.021
6. London ED, Kohno M, Morales AM, Ballard ME. Chronic methamphetamine abuse and corticostriatal deficits revealed by neuroimaging. Brain Res. 2015;1628(Pt A):174–85. doi:10.1016/j.brainres.2014.10.044
7. Koob GF, Volkow ND. Neurobiology of addiction: A neurocircuitry analysis. Lancet Psychiatry. 2016;3(8):760–73. doi:10.1016/S2215-0366(16)00104-8
8. Sutherland MT, McHugh MJ, Pariyadath V, Stein EA. Resting state functional connectivity in addiction: Lessons learned and a road ahead. Neuroimage. 2012;62(4):2281–95. doi:10.1016/j.neuroimage.2012.01.117
9. Tolomeo S, Yu R. Brain network dysfunctions in addiction: a meta-analysis of resting-state functional connectivity. Transl Psychiatry. 2022 Dec 1;12(1). doi:10.1038/s41398-022-01792-6 PubMed PMID: 35091540.
10. Zilverstand A, Huang AS, Alia-Klein N, Goldstein RZ. Neuroimaging impaired response inhibition and salience attribution in human drug addiction: A systematic review. Neuron. 2018;98(5):886–903. doi:10.1016/j.neuron.2018.03.048
11. Bullmore E, Sporns O. Complex brain networks: Graph theoretical analysis of structural and functional systems. Nat Rev Neurosci. 2009;10(3):186–98. doi:10.1038/nrn2575
12. Bassett DS, Sporns O. Network neuroscience. Nat Neurosci. 2017;20(3):353–64. doi:10.1038/nn.4502
13. Sporns O. Networks of the Brain. Networks of the Brain. Cambridge, MA: MIT Press; 2011.
14. Rubinov M, Sporns O. Complex network measures of brain connectivity: Uses and interpretations. Neuroimage. 2010;52(3):1059–69. doi:https://doi.org/10.1016/j.neuroimage.2009.10.003
15. Fornito A, Zalesky A, Breakspear M. Graph analysis of the human connectome: Promise, progress, and pitfalls. Neuroimage. 2013;80:426–44. doi:10.1016/j.neuroimage.2013.04.087
16. Fornito A, Zalesky A, Bullmore ET. Fundamentals of Brain Network Analysis [Internet]. London: Academic Press; 2016. Available from: https://www.elsevier.com/books/fundamentals-of-brain-network-analysis/fornito/978-0-12-407908-3

17. Honey CJ, Sporns O, Cammoun L, Gigandet X, Thiran JP, Meuli R, et al. Predicting human resting-state functional connectivity from structural connectivity. In: Proceedings of the National Academy of Sciences [Internet]. 2009. p. 2035–40. Available from: https://doi.org/10.1073/pnas.0811168106 doi:10.1073/pnas.0811168106
18. Suárez LE, Markello RD, Betzel RF, Mišić B. Linking structure and function in macroscale brain networks. Trends Cogn Sci. 2020;24(4):302–15. doi:10.1016/j.tics.2020.01.008
19. Preti MG, Van De Ville D. Decoupling of brain function from structure reveals regional behavioral specialization in humans. Nat Commun. 2019;10:4747. doi:10.1038/s41467-019-12765-7
20. Biswal B, Zerrin Yetkin F, Haughton VM, Hyde JS. Functional connectivity in the motor cortex of resting human brain using echo-planar MRI. Magn Reson Med. 1995;34(4):537–41. doi:10.1002/mrm.1910340409
21. Fox MD, Raichle ME. Spontaneous fluctuations in brain activity observed with functional magnetic resonance imaging. Nat Rev Neurosci. 2007;8(9):700–11. doi:10.1038/nrn2201
22. A VDKR, Hedden T, Venkataraman A, Evans KC, Lazar SW, Buckner RL. Intrinsic functional connectivity as a tool for human connectomics: theory, properties, and optimization. J Neurophysiol. 2010;103(1):297–321. doi:10.1152/jn.00783.2009
23. Smith SM, Miller KL, Salimi-Khorshidi G, Webster M, Beckmann CF, Nichols TE, et al. Network modelling methods for fMRI. Neuroimage. 2011;54(2):875–91. doi:10.1016/j.neuroimage.2010.08.063
24. Whitfield-Gabrieli S, Nieto-Castanon A. Conn: A functional connectivity toolbox for correlated and anticorrelated brain networks. Brain Connect. 2012;2(3):125–41. doi:10.1089/brain.2012.0073
25. Hutchison RM, Womelsdorf T, Allen EA, Bandettini PA, Calhoun VD, Corbetta M, et al. Dynamic functional connectivity: Promise, issues, and interpretations. Neuroimage. 2013;80:360–78. doi:https://doi.org/10.1016/j.neuroimage.2013.05.079
26. Preti MG, Bolton TAW, Van De Ville D. The dynamic functional connectome: State-of-the-art and perspectives. Neuroimage. 2017;160:41–54. doi:10.1016/j.neuroimage.2016.12.061
27. Lurie DJ, Kessler D, Bassett DS, Betzel RF, Breakspear M, Kheilholz S, et al. Questions and controversies in the study of time-varying functional connectivity in resting fMRI. Network Neuroscience. 2020;4(1):30–69. doi:10.1162/netn_a_00116
28. Allen EA, Damaraju E, Plis SM, Erhardt EB, Eichele T, Calhoun VD. Tracking whole-brain connectivity dynamics in the resting state. Cerebral Cortex. 2014;24(3):663–76. doi:10.1093/cercor/bhs352
29. Calhoun VD, Miller R, Pearlson G, Adalı T. The chronnectome: Time-varying connectivity networks as the next frontier in fMRI data discovery. Neuron. 2014;84(2):262–74. doi:10.1016/j.neuron.2014.10.015
30. Beckmann CF, DeLuca M, Devlin JT, Smith SM. Investigations into resting-state connectivity using independent component analysis. Philosophical Transactions of the Royal Society B: Biological Sciences. 2005;360(1457):1001–13. doi:10.1098/rstb.2005.1634
31. Mattick RP, Breen C, Kimber J, Davoli M. Methadone maintenance therapy versus no opioid replacement therapy for opioid dependence. Cochrane Database of Systematic Reviews. John Wiley and Sons Ltd; 2009. doi:10.1002/14651858.CD002209.pub2 PubMed PMID: 19588333.
32. Sordo L, Barrio G, Bravo MJ, Indave BI, Degenhardt L, Wiessing L. Mortality risk during and after opioid substitution treatment: systematic review and meta-analysis of cohort studies. BMJ. 2017;357:j1550. doi:10.1136/bmj.j1550
33. Chan B, Freeman M, Kondo K, Ayers C, Montgomery J, Paynter R. Pharmacotherapy for methamphetamine/amphetamine use disorder - a systematic review and meta-analysis. Addiction. 2019;114(12):2122–36. doi:10.1111/add.14755
34. Trivedi MH, Walker R, Ling W, A DC, Sharma G, Carmody T. Bupropion and naltrexone in methamphetamine use disorder. N Engl J Med. 2021;384(2):140–53. doi:10.1056/NEJMoa2020214
35. Woo CW, Chang LJ, Lindquist MA, Wager TD. Building better biomarkers: Brain models in translational neuroimaging. Nat Neurosci. 2017;20(3):365–77. doi:10.1038/nn.4478

36. Members CGC, Team A, Team A, Team I. The ASAM/AAAP Clinical Practice Guideline on the Management of Stimulant Use Disorder. J Addict Med. 2024;18(1S Suppl 1):1–56. doi:10.1097/ADM.0000000000001299
37. Ford BR, Bart G, Grahan B, Shearer RD, Winkelman TNA. Associations Between Polysubstance Use Patterns and Receipt of Medications for Opioid Use Disorder Among Adults in Treatment for Opioid Use Disorder. J Addict Med. 2021;15(2):159–62. doi:10.1097/ADM.0000000000000726
38. Bunting AM, Krawczyk N, Choo TH, Pavlicova M, McNeely J, Tofighi B. Polysubstance use before and during treatment with medication for opioid use disorder: Prevalence and association with treatment outcomes. J Subst Abuse Treat. 2022;143:108830. doi:10.1016/j.jsat.2022.108830
39. Cui Z, Hayashi K, Bach P, Milloy MJ, Kerr T. Crystal methamphetamine use and methadone maintenance treatment dissatisfaction: A prospective cohort study in Vancouver, Canada. Journal of Substance Use and Addiction Treatment. 2023 Aug 1;151:208956. doi:10.1016/J.JOSAT.2023.208956
40. Russell C, Law J, Imtiaz S, Rehm J, B LF, Ali F. The impact of methamphetamine use on medications for opioid use disorder treatment retention: a scoping review. Addict Sci Clin Pract. 2023;18(1):48. doi:10.1186/s13722-023-00402-0
41. Calhoun VD, Sui J. Multimodal fusion of brain imaging data: A key to finding the missing link(s) in complex mental illness. Biol Psychiatry Cogn Neurosci Neuroimaging. 2016;1(3):230–44. doi:10.1016/j.bpsc.2015.12.005
42. Sui J, Adalı T, Yu Q, Chen J, Calhoun VD. A review of multivariate methods for multimodal fusion of brain imaging data. J Neurosci Methods. 2012;204(1):68–81. doi:10.1016/j.jneumeth.2011.10.031
43. Sui J, He H, Pearlson GD, Adali T, Kiehl KA, Yu Q. Three-way (N-way) fusion of brain imaging data based on mCCA+jICA and its application to discriminating schizophrenia. Neuroimage. 2013;68:119–32. doi:10.1016/j.neuroimage.2012.11.051
44. Sui J, He H, Yu Q, Chen J, Rogers J, Pearlson GD. Combination of resting state fMRI, DTI, and sMRI data to discriminate schizophrenia by N-way MCCA+jICA. Front Hum Neurosci. 2013;7:235. doi:10.3389/fnhum.2013.00235
45. Qi S, Calhoun VD, van Erp TGM, Bustillo J, Damaraju E, Turner JA, et al. Multimodal fusion with reference: Searching for joint neuromarkers of working memory deficits in schizophrenia. IEEE Trans Med Imaging. 2018;37(1):93–105. doi:10.1109/TMI.2017.2725306
46. Arbabshirani MR, Plis S, Sui J, Calhoun VD. Single subject prediction of brain disorders in neuroimaging: Promises and pitfalls. Neuroimage. 2017;145(Pt B):137–65. doi:10.1016/j.neuroimage.2016.02.079
47. Varoquaux G, Raamana PR, Engemann DA, Hoyos-Idrobo A, Schwartz Y, Thirion B. Assessing and tuning brain decoders: Cross-validation, caveats, and guidelines. Neuroimage. 2017;145(Pt B):166–79. doi:10.1016/j.neuroimage.2016.10.038
48. Poldrack RA, Huckins G, Varoquaux G. Establishment of best practices for evidence for prediction: A review. JAMA Psychiatry. 2020;77(5):534–40. doi:10.1001/jamapsychiatry.2019.3671
49. Bzdok D, Meyer-Lindenberg A. Machine learning for precision psychiatry: Opportunities and challenges. Biol Psychiatry Cogn Neurosci Neuroimaging. 2018;3(3):223–30. doi:10.1016/j.bpsc.2017.11.007
50. Bzdok D, Ioannidis JPA. Exploration, inference, and prediction in neuroscience and biomedicine. Trends Neurosci. 2019;42(4):251–62. doi:10.1016/j.tins.2019.02.001
51. Yarkoni T, Westfall J. Choosing prediction over explanation in psychology: lessons from machine learning. Perspect Psychol Sci. 2017;12(6):1100–22. doi:10.1177/1745691617693393
52. Chen T, Guestrin C. XGBoost: A scalable tree boosting system. In: Proceedings of the 22nd ACM SIGKDD International Conference on Knowledge Discovery and Data Mining [Internet]. 2016. Available from: https://doi.org/10.1145/2939672.2939785 doi:10.1145/2939672.2939785
53. Lundberg SM, Lee SI. A unified approach to interpreting model predictions. Adv Neural Inf Process Syst [Internet]. 2017;30:4765–74. Available from: https://papers.nips.cc/paper_files/paper/2017/hash/8a20a8621978632d76c43dfd28b67767-Abstract.html
54. Benjamini Y, Hochberg Y. Controlling the false discovery rate: A practical and powerful approach to multiple testing. Journal of the Royal Statistical Society: Series B. 1995;57(1):289–300. doi:10.1111/j.2517-6161.1995.tb02031.x

55. Kay SR, Fiszbein A, Opler LA. The Positive and Negative Syndrome Scale (PANSS) for schizophrenia. Schizophr Bull. 1987;13(2):261–76. doi:10.1093/schbul/13.2.261
56. Keefe RSE, Goldberg TE, Harvey PD, Gold JM, Poe MP, Coughenour L. The Brief Assessment of Cognition in Schizophrenia: Reliability, sensitivity, and comparison with a standard neurocognitive battery. Schizophr Res. 2004;68(2–3):283–97. doi:10.1016/j.schres.2003.09.011
57. Whitfield-Gabrieli S, Nieto-Castanon A. Conn: A functional connectivity toolbox for correlated and anticorrelated brain networks. Brain Connect. 2012;2(3):125–41. doi:10.1089/brain.2012.0073
58. Nieto-Castanon A, Whitfield-Gabrieli S. CONN functional connectivity toolbox: RRID SCR_009550, release 22. CONN functional connectivity toolbox: RRID SCR_009550, release 22. Hilbert Press; 2022. doi:10.56441/hilbertpress.2246.5840
59. Power JD, Barnes KA, Snyder AZ, Schlaggar BL, Petersen SE. Spurious but systematic correlations in functional connectivity MRI networks arise from subject motion. Neuroimage. 2012;59(3):2142–54. doi:10.1016/j.neuroimage.2011.10.018
60. Power JD, Mitra A, Laumann TO, Snyder AZ, Schlaggar BL, Petersen SE. Methods to detect, characterize, and remove motion artifact in resting-state fMRI. Neuroimage. 2014;84:320–41. doi:10.1016/j.neuroimage.2013.08.048
61. Satterthwaite TD, Elliott MA, Gerraty RT, Ruparel K, Loughead J, Calkins ME. An improved framework for confound regression and filtering for control of motion artifact in resting-state functional connectivity. Neuroimage. 2013;64:240–56. doi:10.1016/j.neuroimage.2012.08.052
62. Ciric R, Wolf DH, Power JD, Roalf DR, Baum GL, Ruparel K. Benchmarking of participant-level confound regression strategies for the control of motion artifact in studies of functional connectivity. Neuroimage. 2017;154:174–87. doi:10.1016/j.neuroimage.2017.03.020
63. Behzadi Y, Restom K, Liau J, Liu TT. A component based noise correction method, CompCor, for BOLD and perfusion based fMRI. Neuroimage. 2007;37(1):90–101. doi:10.1016/j.neuroimage.2007.04.042
64. Behrens TEJ, Berg HJ, Jbabdi S, Rushworth MFS, Woolrich MW. Probabilistic diffusion tractography with multiple fibre orientations: What can we gain? Neuroimage. Vol. 34. 2007;34(1):144–55. doi:10.1016/j.neuroimage.2006.09.018
65. Hagmann P, Cammoun L, Gigandet X, Meuli R, Honey CJ, Wedeen VJ, et al. Mapping the structural core of human cerebral cortex. PLoS Biol. 2008;6(7):e159. doi:10.1371/journal.pbio.0060159
66. Jones DK, Knösche TR, Turner R. White matter integrity, fiber count, and other fallacies: The do's and don'ts of diffusion MRI. Neuroimage. 2013;73:239–54. doi:10.1016/j.neuroimage.2012.06.081
67. Maier-Hein KH, Neher PF, Houde JC, Côté MA, Garyfallidis E, Zhong J, et al. The challenge of mapping the human connectome based on diffusion tractography. Nat Commun. 2017;8:1349. doi:10.1038/s41467-017-01285-x
68. Hyvarinen A. Fast and robust fixed-point algorithms for independent component analysis. IEEE Trans Neural Netw. 1999;10(3):626–34. doi:10.1109/72.761722
69. Smith SM, Fox PT, Miller KL, Glahn DC, Fox PM, Mackay CE. Correspondence of the brain's functional architecture during activation and rest. Proc Natl Acad Sci U S A. 2009;106(31):13040–5. doi:10.1073/pnas.0905267106
70. Allen EA, Erhardt EB, Damaraju E, Gruner W, Segall JM, Silva RF. A baseline for the multivariate comparison of resting-state networks. Front Syst Neurosci. 2011;5:2. doi:10.3389/fnsys.2011.00002
71. Griffanti L, Douaud G, Bijsterbosch J, Evangelisti S, Alfaro-Almagro F, Glasser MF. Hand classification of fMRI ICA noise components. Neuroimage. 2017;154:188–205. doi:10.1016/j.neuroimage.2016.12.036
72. Rubinov M, Sporns O. Complex network measures of brain connectivity: Uses and interpretations. Neuroimage. 2010;52(3):1059–69. doi:10.1016/j.neuroimage.2009.10.003
73. Fornito A, Zalesky A, Breakspear M. Graph analysis of the human connectome: Promise, progress, and pitfalls. Neuroimage. 2013;80:426–44. doi:10.1016/j.neuroimage.2013.04.087
74. Beard CL, Schmitz JM, Soder HE, Suchting R, Yoon JH, Hasan KM. Regional differences in white matter integrity in stimulant use disorders: a meta-analysis of diffusion tensor imaging studies. Drug Alcohol Depend. 2019;201:29–37.

doi:10.1016/j.drugalcdep.2019.03.023

75. Gong MQ, Shen YX, Liang WB, Zhang Z, He CX, Lou MW. Impairments in the default mode and executive networks in methamphetamine users during short-term abstinence. Int J Gen Med. 2022;15:6073–84. doi:10.2147/IJGM.S369571
76. Li X, Su H, Zhong N, Chen T, Du J, Xiao K, et al. Aberrant Resting-State Cerebellar-Cerebral Functional Connectivity in Methamphetamine-Dependent Individuals After Six Months Abstinence. Front Psychiatry. 2020 Mar 31;11. doi:10.3389/fpsyt.2020.00191
77. Jiang P, Sun J, Zhou X, Lu L, Li L, Xu J, et al. Dynamics of intrinsic whole-brain functional connectivity in abstinent males with methamphetamine use disorder. Drug and Alcohol Dependence Reports. 2022 Jun;3:100065. doi:10.1016/j.dadr.2022.100065
78. Ieong HFH, Yuan Z, Yang Z, Wang Y. Resting-state neuroimaging and neuropsychological findings in opioid-dependent patients during methadone maintenance treatment: A literature review. Front Hum Neurosci. 2017;11:169. doi:10.3389/fnhum.2017.00169
79. Li W, Li Q, Wang Y, Zhu J, Ye J, Yan X, et al. Methadone-induced damage to white matter integrity in methadone maintenance patients: A longitudinal self-control DTI study. Sci Rep. 2016;6:19662. doi:10.1038/srep19662
80. Chen J, Li Y, Wang S, Li W, Liu Y, Jin L, et al. Methadone maintenance treatment alters couplings of default mode and salience networks in individuals with heroin use disorder: A longitudinal self-controlled resting-state fMRI study. Front Psychiatry [Internet]. 2023;Volume 14-2023. Available from: https://www.frontiersin.org/journals/psychiatry/articles/10.3389/fpsyt.2023.1132407
81. Xue J, Chen J, Wang S, Li W, Zhu J, Wang F, et al. Assessing brain activity in male heroin-dependent individuals under methadone maintenance treatment: A resting-state fMRI study. Psychiatry Res Neuroimaging. 2022 Mar 1;320:111431. doi:10.1016/J.PSCYCHRESNS.2021.111431 PubMed PMID: 35007942.
82. Zhu J, Wang S, Liu Y, Wang F, Li Q, Li Z, et al. The influence of methadone on cerebral gray matter and functional connectivity. Ann Palliat Med. 2021 Sep 1;10(9):9497–507. doi:10.21037/apm-21-2012 PubMed PMID: 34628875.
83. Herlinger K, Lingford-Hughes A, Reed LJ. Opioid use disorder and the brain: A clinical perspective. Addiction. 2022;117(2):495–507. doi:10.1111/add.15636
84. Ieong HF, Yuan Z. Resting-state neuroimaging and neuropsychological findings in opioid use disorder during abstinence: A review. Front Hum Neurosci. 2017;11:169. doi:10.3389/fnhum.2017.00169

Figures

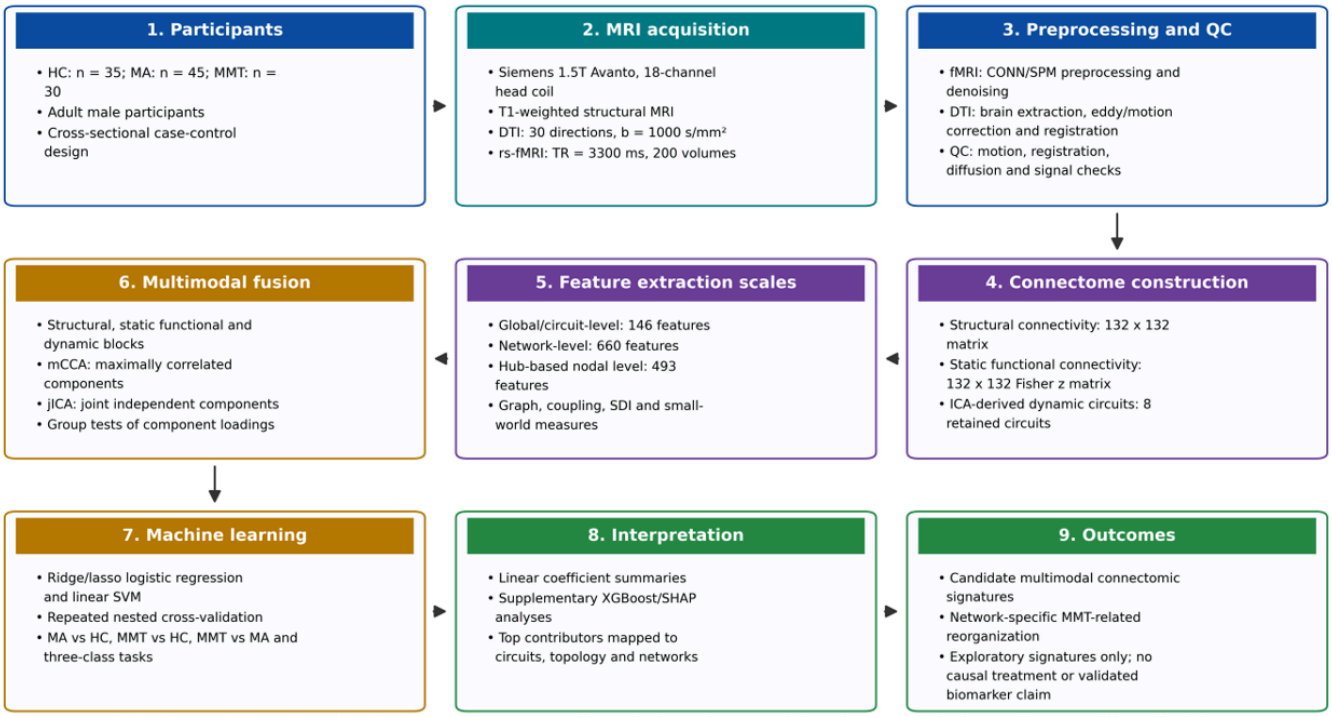
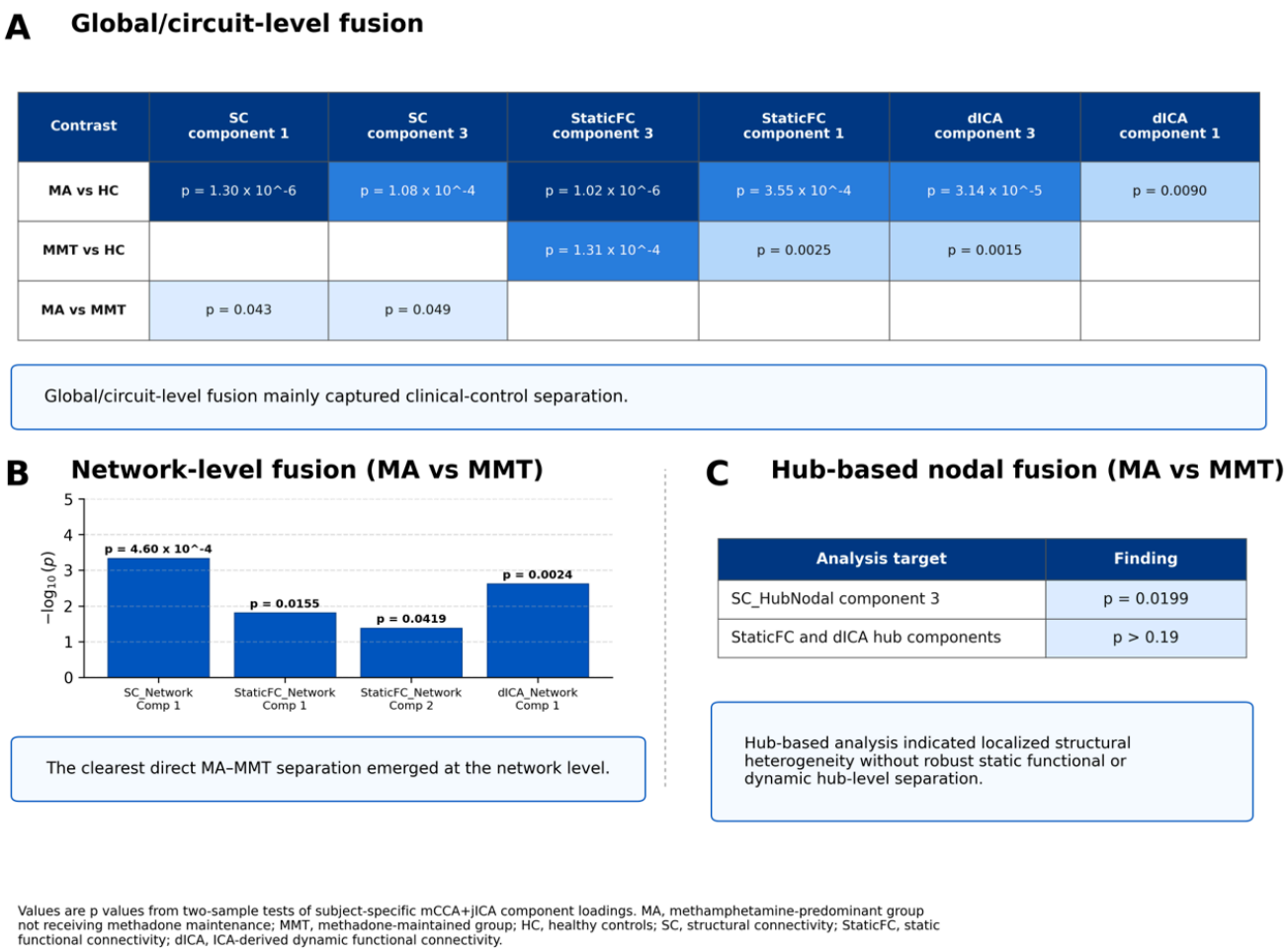


Figure 1

Overview of the multiscale multimodal connectomic analysis pipeline, from participant grouping and multimodal magnetic resonance imaging acquisition to preprocessing, connectome construction, multiscale feature extraction, fusion, machine-learning evaluation, interpretation, and outcome-level inference.



Values are p values from two-sample tests of subject-specific mCCA+jICA component loadings. MA, methamphetamine-predominant group not receiving methadone maintenance; MMT, methadone-maintained group; HC, healthy controls; SC, structural connectivity; StaticFC, static functional connectivity; dICA, ICA-derived dynamic functional connectivity.

Figure 2

Multimodal mCCA+jICA component-loading group differences across global/circuit-level, network-level, and hub-based scales. Values are p values from two-sample tests of component loadings. Network-level and hub-based component tests were available for the MA versus MMT contrast in the uploaded outputs.

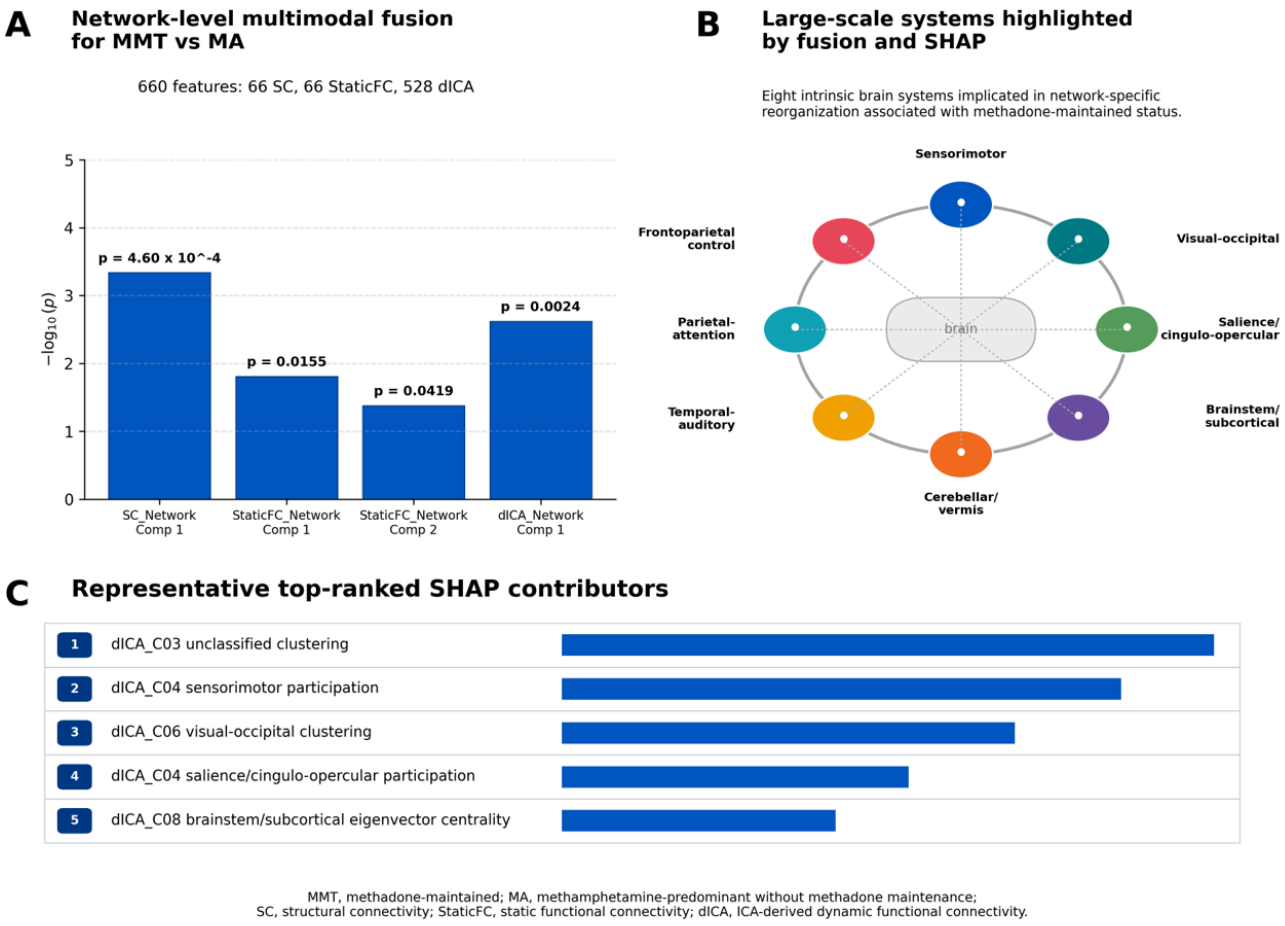


Figure 3

Network-level multimodal fusion and SHAP interpretation identify functional and dynamic reorganization associated with methadone-maintained status. The figure highlights dICA- and graph-derived network contributors to the MMT versus MA contrast.

A Primary machine-learning classification performance

Contrast	Best feature scale	Best model	Accuracy	Balanced accuracy	Sensitivity	Specificity	F1	AUC
MA vs HC	Network-level	Ridge logistic regression	0.983	0.982	0.993	0.971	0.986	1.000
MMT vs HC	Combined multiscale	Ridge logistic regression	0.964	0.964	0.967	0.962	0.962	0.983
MMT vs MA	Network-level	Ridge logistic regression	0.662	0.643	0.544	0.741	0.550	0.694

B Three-class classification summary

Best feature scale	Combined multiscale
Best model	Ridge multinomial logistic regression
Accuracy	0.755
Balanced accuracy	0.735
F1	0.729 macro
AUC	Not reported
CV folds	15

Takeaway

Clinical-control contrasts outperformed the direct MMT vs MA contrast.

MA, methamphetamine-predominant; MMT, methadone-maintained; HC, healthy controls.

Figure 4

Primary machine-learning classification performance. Clinical-control classification was stronger than direct MMT versus MA classification, supporting a shared methamphetamine-predominant connectomic background with subtler network-specific clinical-group differences.

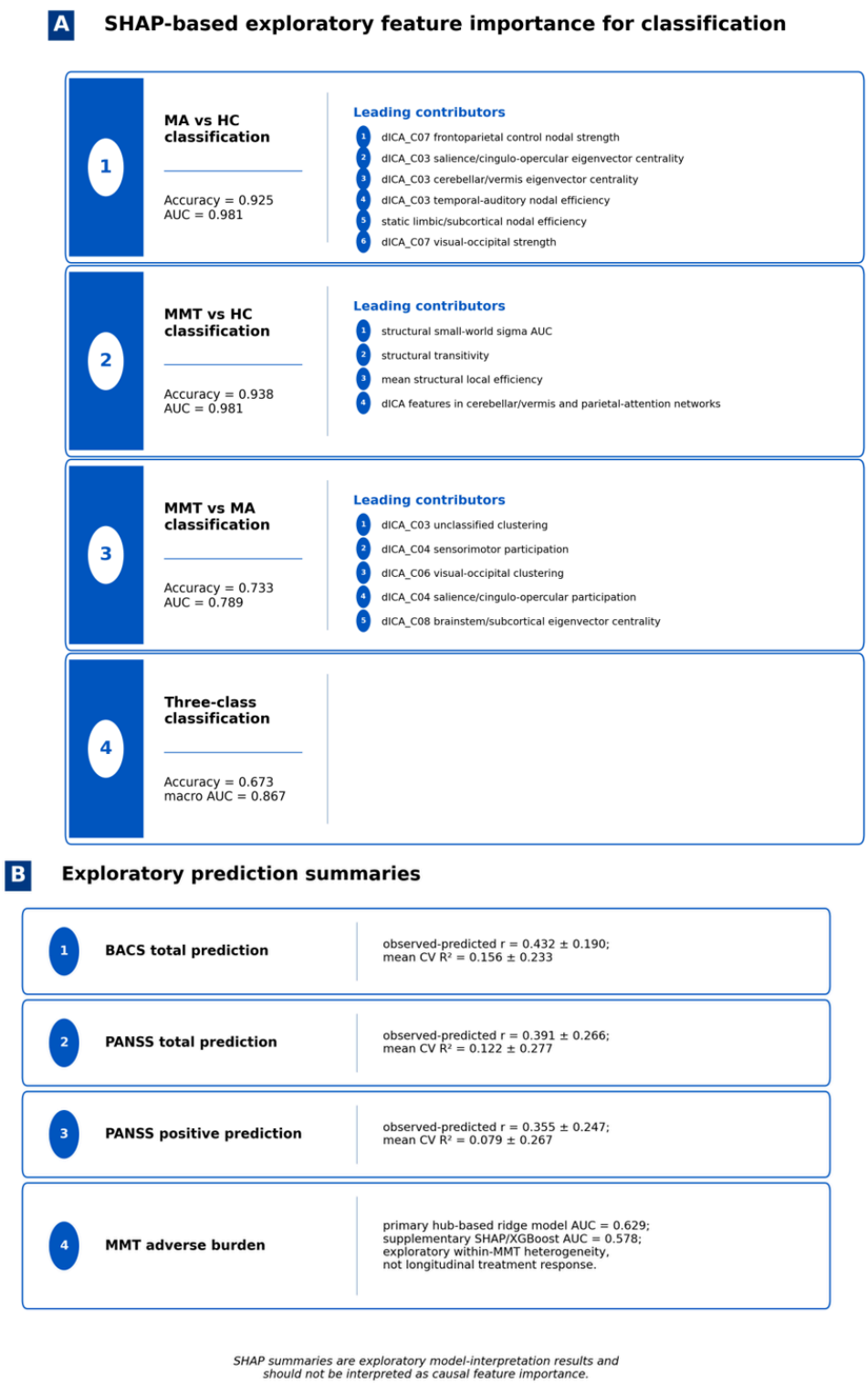


Figure 5

SHAP-based exploratory feature importance across classification and prediction models. Top features emphasize ICA-derived dynamic circuits, structural topology, and large-scale networks including salience/cingulo-opercular, frontoparietal, cerebellar/vermis, temporal-auditory, visual-occipital, sensorimotor, and brainstem/subcortical systems.

Supplementary Files

This is a list of supplementary files associated with this preprint. Click to download.

- SupplementaryMaterial.docx